Check for updates

An improved prediction model for COD measurements using UV-Vis spectroscopy

Li Guan, [ID] *[a] Yijun Zhou[b] and Sen Yang[a]

In the 21st century, although water quality has been improved in the last two decades, water pollution by organic contaminants has remained a non-negligible issue in China, so Chemical-Oxygen Demand (abbreviated as COD, unit: mg L^{-1}) is often used as the main index to measure the degree of surface water pollution. UV-Vis spectroscopy, as a sensitive and rapid analytical technique, is a green detection technology suitable for automatic online COD detection equipment. However, due to the complex composition of surface water, the interference degree of the UV-Vis spectrum caused by turbidity is strongly correlated with the size, type and color of particulate matter in the solution, which results in noise sensitivity and poor generalization of the current detection model. Therefore, the main purpose of this research is to improve the traditional detection model performance by using deep learning and a spectrum preprocessing algorithm. Firstly, we used an improved noise filter based on discrete wavelet transforms to solve the noise sensitivity. Secondly, we proposed a novel COD detection network to address poor generalization. Thirdly, we collected a total of 2259 water samples' UV-Vis absorption spectra and corresponding COD as a dataset. Then, we pipelined the improved noise removal algorithm and proposed COD detection network, as a complete COD prediction model. Finally, the experiment on the dataset shows that the COD prediction model has a good performance in terms of both noise tolerance and accuracy.

1. Introduction

According to the "Communique on the State of China's Environment 2022",[1] as shown in Fig. 1, among 1731 water quality monitors in 2022, the proportion of class "I" (drinkable) to class "III" (mild contamination) is 74.9%, 3.9 percent higher than in 2021. Class "VI" (inferior) accounted for 3.4%, 3.3 percent lower than in 2021.

In the 21st century, despite China's rapid economic development, environmental problems are still serious, especially surface water pollution. Although water quality has been improved in the last two decades, water pollution by organic contaminants has remained a non-negligible issue, so Chemical-Oxygen Demand (abbreviated as COD, unit: mg L^{-1}) is often used as the main index to measure the degree of surface water pollution.[2,3]

For COD detection, the relatively mature methods in the academic field are the traditional chemical method, electrochemical method and molecular spectroscopy.

Among these methods, the traditional method based on wet chemistry, which is the national standard COD measurement

method, has the disadvantage of adding toxic chemicals (*e.g.* mercurate, dichromate, *etc.*) and is time consuming (requiring 2–4 h). Therefore, it is urgent to seek a rapid, high-precision and pollution-free technology for COD measurement to realize online surface water quality detection. On the other hand, molecular spectroscopy[4,5] is an analytical method based on the Ultraviolet-Visible spectrum (abbreviated as UV-Vis). As a sensitive and rapid analytical technique, it has been widely recognized in the field of physical evidence analysis for decades. On the other hand, UV-Vis spectroscopy is also a green detection technology suitable for automatic online COD detection equipment. Compared with other COD measurement methods, UV-Vis spectroscopy has the characteristics of no pollution, low cost and short cycle and low detection accuracy, which makes this method attract wide attention in the field of COD detection of surface water.[6,7]

Agustsson *et al.*[8] used the UV-Vis full band absorption spectrum to detect COD in surface water and modeled it based on Least Squares Vector Machine (abbreviated as LS-SVM). Experiments showed that this method has higher model generalization ability than Partial Least Squares (abbreviated as PLS). Wang *et al.*[9] described the use of deep learning technologies in the prediction of COD for urban sewage. Additionally, the use of convolutional neural networks (CNNs) to process the one-dimensional spectrum was encouraged. Deep learning-based models were also described by Jiang *et al.*[10] for the

[a]Industrial Perception and Intelligent Manufacturing Equipment Engineering Research Center of Jiangsu Province, Nanjing Vocational University of Industry Technology, Nanjing 210023, China. E-mail: li.guan.nangong@foxmail.com

[b]Department of Data Analysis, Nanjing Weiwo Software Technology Co., Ltd, Nanjing, 210012, P. R. China
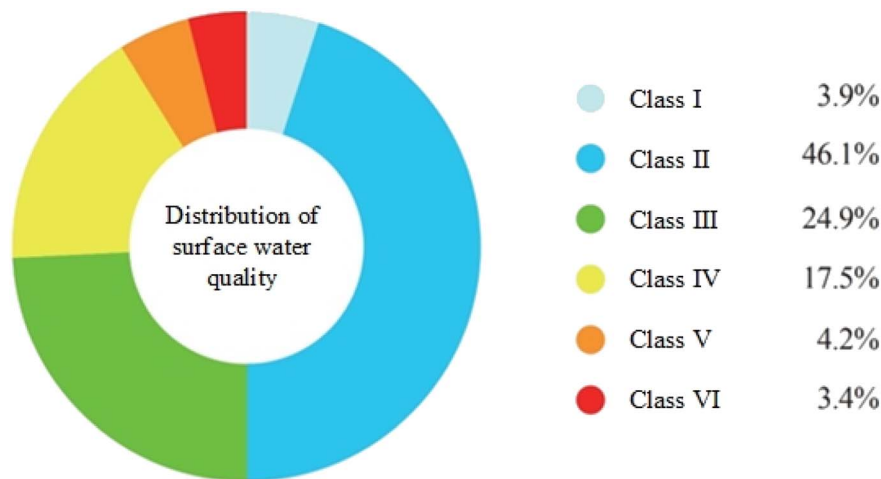
Fig. 1 Surface water quality in China in 2022.

multi-source data fusion to dynamically predict the water quality of an urban sewer.

However, due to the complex composition of surface water, the interference degree of the UV-Vis spectrum caused by turbidity is strongly correlated with the size, type and color of particulate matter in the solution, which results in poor consistency between the COD detection model in the laboratory environment and the real scenario.[11,12] Therefore, a large number of revisions are always needed after spectrum acquisition, which makes the spectrum preprocessing of the model very complicated and tedious.[13]

In this paper, the research status of COD detection is reviewed. The main purpose of this research is to improve the traditional detection model performance by using deep learning and a spectrum preprocessing algorithm. The focus is on the utilization of deep learning combined with spectral preprocessing algorithms as a general method for COD detection.

The limitations of the current detection model, such as noise sensitivity and poor generalization, are addressed by proposing the use of an improved discrete wavelet transforms (DWT) based noise filter and well pretrained detection network. The main contributions of this work are:

1. Based on DWT, an adaptive soft threshold filter is proposed for the spectrum characteristics of real water samples, which can better remove noise and preserve features.

2. Through a large amount of water samples collection, a total of 2259 water samples' UV-Vis absorption spectra and corresponding COD have been collected, which is now open access and continuously updating.

3. Inspired by computer vision model, a COD detection network based on one-dimensional convolutional module and convolutional block attention module (CBAM) is proposed. The experiment shows that if the network is trained from the per-tained weights, the relative error of 90.36% prediction results is within 5%, and that of 99.54% COD prediction results is within 10%.

4. Pipelined the improved noise removal algorithm and proposed COD detection network, and as a complete COD prediction model, they have a good performance on both noise tolerance and accuracy. The experiment shows that the Pearson correlation coefficient between the ground truth and the prediction has a value of 0.97.

The paper has been organized as follows: Section 2 describes the detailed technique of proposed detection methods, Section 3 shows the training process and generalization of the model, Section 4 discusses the model performance comparison of multiple algorithms and Section 5 draws the conclusion in this work.

2. Materials and methods

2.1 Water samples collection

Considering the transportation environment of water samples and the time required for chemical digestion, most collection points are set as surrounding surface waters, including Qian Lake, QinHuai River, XuanWu Lake, SanQ Wetland, LiShui River, Yang-Shan Lake, XuPu River and MengJiaG River. A total of 2970 groups of water samples were collected. UV-Vis absorption spectrum were collected by spectrometers in laboratory environment, background and reference absorption spectrum were deducted.

However, due to the proximity of individual collection points, the absorption spectrum of some water samples completely overlaps, and these samples cannot provide information gain for subsequent modeling. Therefore, after removing highly overlapping samples, the remaining number of effective samples is 2259 groups. The collection points and distribution of COD values is shown in Table 1.

2.2 Standard COD determination

The true value of COD in water samples is obtained by rapid digestion spectrophotometric method (HJ/T399-2007), which can be regarded as ground-truth.

Table 1 COD distribution at each water sampling location

Location	Mean (mg L^{-1})	SD	Min (mg L^{-1})	Q1 (mg L^{-1})	Median (mg L^{-1})	Q3 (mg L^{-1})	Max (mg L^{-1})	Data size
Qian Lake	5.9	1.21	3.68	5.46	6.08	6.7	7.21	228
QinHuai River	3.9	2.26	0.95	2.22	3.71	5.8	6.64	349
XuanWu Lake	3.99	2.39	0.8	2.4	4.43	5.69	6.65	241
SanQ Wetland	3.34	1.81	0.85	2.04	3.56	4.8	5.35	273
LiShui River	3.72	1.58	1.35	2.66	4.18	4.89	5.31	286
YangShan Lake	3.84	1.5	1.74	2.95	4.16	5.01	5.35	238
XuPu River	3.52	1.57	0.92	2.29	3.73	4.81	5.31	364
MengJiaG River	3.82	2.33	0.57	1.36	4.43	5.69	6.83	280

2.3 UV-Vis absorption spectrum acquisition

The light intensity map of water sample under the current light source was obtained by means of spectrograph, and the light intensity diagram of blank liquid (generally using distilled water) is compared to calculate the corresponding absorbance of each wavelength, Finally, the absorption spectrum of UV-Vis can be obtained by taking wavelength as abscissa and absorbance as ordinate. The collection method and equipment are shown in Fig. 2(A).

2.4 The characteristic of samples spectrum

UV-Vis absorption spectrogram of a water sample randomly selected from the dataset are shown in Fig. 2(B). As can be seen from the figure, there is high-frequency noise (in the form of jitter and spikes) uniformly distributed in the whole band (194–699 nm). The noise form is random and instantaneous value follows Gaussian distribution, which requires the subsequent COD prediction network to have high robustness.

2.5 Noise removal

Accurate prediction of COD requires the input UV-Vis absorption spectrum with high signal-to-noise ratio. To achieve this, this work applies a discrete wavelet transform (DWT) based filter to remove high-frequency noise from the spectrum.

As a mathematical method to decompose signals into different frequency groups, DWT provides an effective method for analyzing non-stationary signals and has been widely studied. The DWT of signal $x(t)$ can be defined as formula (1):[14,15]

$$\text{DWT}(j,k) = \frac{1}{\sqrt{2^j}} \int_{-\infty}^{+\infty} x(t)\psi^*\left(\frac{t-k2^j}{2^j}\right)\mathrm{d}t \qquad (1)$$

where $\psi(t)$ is the mother wavelet, '*' represents the complex conjugate, j and $k(j, k \in R)$ are two scaling factors. j determines oscillator frequency and the length of wavelet, k determines shifted position.

Implement of DWT filter in this work is based on three steps:

Step 1: DWT decomposition of the UV-Vis absorption spectrum by using formula (2):

$$x(t) = \sum_{k=0}^{2^{N-j}-1} a_{j,k} 2^{-\frac{j}{2}}\phi(2^{-j}t-k) + \sum_{j=1}^{J}\sum_{k=0}^{2^{N-j}-1} d_{j,k} 2^{-\frac{j}{2}}\psi(2^{-j}t-k) \quad (2)$$

where $J(J \leq N)$ is the number of decomposition level, N is the maximum decomposition level, $a_{j,k}$ is the approximate coefficients at level j, $d_{j,k}$ is the detailed coefficients at level j.

Step 2: Process DWT coefficients of high frequency part by threshold function:

There two well-known threshold function, which is hard threshold function (shown as formula (3)) and soft threshold function (shown as formula (4)).

$$\hat{w}_{j,k} = \begin{cases} w_{j,k} & |w_{j,k}| \geq \lambda \\ 0 & |w_{j,k}| < \lambda \end{cases} \qquad (3)$$

where λ is the threshold (always value as $\sigma_\text{n}\sqrt{2\ln N}$), σ_n represents the variance of noise, N represents the spectrum length, $w_{j,k}$ represents DWT coefficients. The characteristic of the hard threshold method is that the spectrum details such as signal edge can be preserved well.
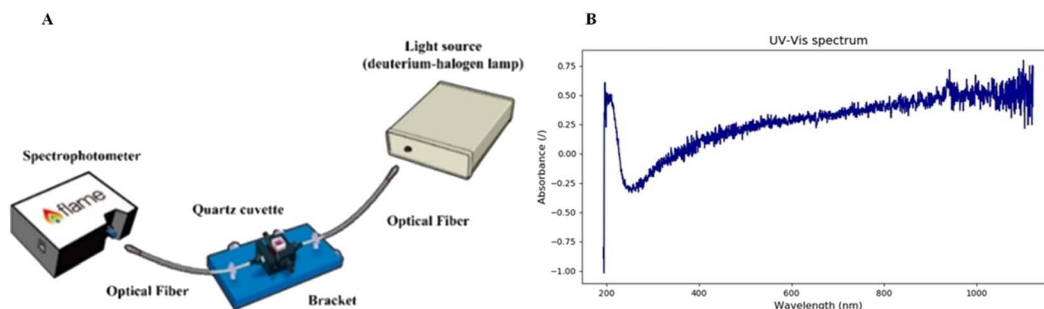

Fig. 2 UV-Vis absorption spectrum acquisition method. (A) Equipment layout diagram. (B) UV-Vis absorption spectrum of a water sample.

$$\hat{w}_{j,k} = \begin{cases} \text{sgn}(w_{j,k})(|w_{j,k}| - \lambda) & |w_{j,k}| \geq \lambda \\ 0 & |w_{j,k}| < \lambda \end{cases} \quad (4)$$

where sgn(.) is the symbolic function. The characteristic of soft threshold method is that the wavelet coefficient estimated by soft threshold method has a constant deviation from that of the original signal. Compared with hard threshold method, soft threshold method can process the signal more smoothly, but it will cause edge blur and other distortion.

Therefore, this work improves the soft threshold function by adaptive to make it have the characteristics of high order smoothing, the improved threshold function is shown as formula (5).

$$\hat{w}_{j,k} = \begin{cases} \text{sgn}(w_{j,k})\left(w_{j,k} - \lambda + \dfrac{\lambda}{\eta + 1}\right) & |w_{j,k}| \geq \lambda \\ \dfrac{w_{j,k}^{\eta+1}}{(\eta + 1)\lambda^{\eta}} & |w_{j,k}| < \lambda \end{cases} \quad (5)$$

where, η is a positive integer greater than zero, which plays a role in adjusting the smoothness of the threshold function in the transition region.

Taking $\lambda = 20$ and $\eta = 2$ as examples, the hard threshold function, improved threshold function and soft threshold function are drawn respectively, as shown in Fig. 3(A). It can be seen that the improved soft threshold function is smoother in the transition region than the traditional soft threshold function, and is more consistent with the continuous characteristics of UV-Vis absorption spectrum.

Step 3: UV-Vis absorption spectrum reconstruction based on DWT coefficients.

As mentioned above, the DWT is a two-dimensional time-scale processing method for non-stationary signals with adequate scale values and shifting in time. The wavelet transform is capable of representing signals in different resolutions by dilating and compressing its basis functions.

On the other hand, the UV-Vis spectrum of measured water is often disturbed by low-frequency baseline and high-frequency noise. The low-frequency baseline part is caused by the scattering of particles in the measured water, and can be corrected through multivariate scattering. The high-frequency noise part is mainly caused by the light source, optical path and spectrum detection instrument, and mainly appears as a non-stationary signal that continuously jumps during online measurement. For the high-frequency noise part, we need to use the translation and scaling of wavelet in DWT to calculate the high-frequency coefficients, then filter the high frequency signal through the improved threshold function, and finally reconstruct the spectrum to achieve the removal of high frequency noise while preserving the spectral characteristics.

A raw UV-Vis absorption spectrum selected from the dataset are shown as Fig. 3(C). The de-noising spectrum are shown as Fig. 3(B). As shown in Fig. 3, the proposed adaptive soft threshold function can better remove the jitter and spikes in raw UV-Vis absorption spectrum.

2.6 Data set division

From 2259 groups of water samples, 1900 groups of samples were selected as the training dataset by uniform distribution. In the remaining 359 groups of samples, 200 groups of samples were selected as the validation dataset by uniform distribution. Finally, take remaining 159 groups of water samples as testing dataset.

2.7 Data normalization

At the initial input layer of the network, we normalize the data with Min-Max-Scaler to avoid over-reliance on certain features, while speeding up learning by limiting all variables to a range between 0 and 1. Between convolutional operation and nonlinear activation within the network, we use the BN layer to mitigate gradient explosion and gradient disappearance, and accelerate the convergence of the network.

2.8 Network design

From the microscopic point of view, the essence of light absorption of a substance is the absorption of light energy by electrons. The main reason for the different position of the absorption peak wavelength is that electrons absorb light of
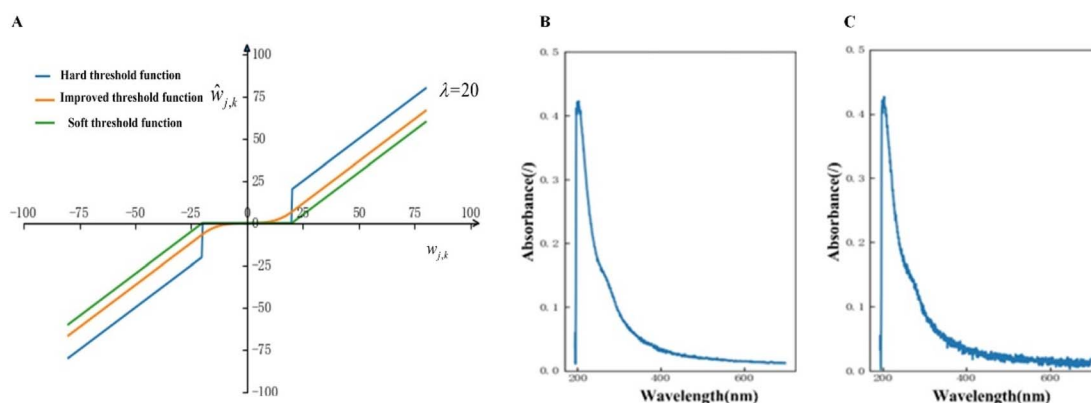

Fig. 3 Improved threshold function and performance of noise removal. (A) Comparison of three threshold functions. (B) The UV-Vis absorption spectrum after de-noising. (C) A raw UV-Vis absorption spectrum selected from the dataset.

different wavelengths according to the different energy levels required by the transition.

This model is implemented as a convolutional neural network. The network architecture is inspired by the YOLO model for object detection.[16–18] To further reduce the complexity of the model. We replace most of fully connected layer with 1×1 convolution kernel. Our network has 17 convolutional layers and 2 attention blocks followed by an adaptive pooling layer and 2 linear layers.

The input of our network is the full band UV-Vis absorption spectrum, and the final output of our network is the 1×1 tensor of COD predictions.

The network structure used in this work is shown in Fig. 4, which mainly includes: convolutional module,[19,20] residual module[21] and Convolutional Block Attention Module (CBAM).[22,23]

For convolutional module, the calculate operation of feature map is shown in formula (6):

$$M_{\text{conv}}(F) = \text{LeakyRelu}(\text{BN}(\text{Conv}(F))) \qquad (6)$$

where 'F' represents the feature map obtained in previous layer, '$\text{Conv}(\cdot)$' is the convolution operation on feature map, '$\text{BN}(\cdot)$'

represents Batch Normalization layer, '$\text{LeakyRelu}(\cdot)$' represents using LeakyReLU as activation function on feature map.

For residual module, the calculate operation of feature map is shown in formula (7):

$$M_{\text{res}}(F) = \text{Conv}_{3\times1}(\text{Conv}_{1\times1}(F)) + F \qquad (7)$$

where '$\text{Conv}_{3\times1}(\cdot)$' is the convolution operation with 3×1 kernel on feature map, '$\text{Conv}_{1\times1}(\cdot)$' is the convolution operation with 1×1 kernel on feature map.

For CBAM, the calculate operation of feature map is shown in formula (8)–(10):

$$M_{\text{CBAM}}(F) = M_{\text{spatial}}(F) \times M_{\text{channel}}(F) \times F \qquad (8)$$

$$M_{\text{spatial}}(F) = \sigma(\text{Conv}_{7\times1}([\text{Avgpool}(F); \text{Maxpool}(F)])) \qquad (9)$$

$$M_{\text{chan}}(F) = \sigma(\text{MLP}(\text{Maxpool}(F)) + \text{MLP}(\text{Avgpool}(F))) \qquad (10)$$

where '$M_{\text{spatial}}(\cdot)$' represents spatial-wise weights tensor obtained by spatial attention module, '$M_{\text{chan}}(F)$' represents channel-wise weights tensor obtained by spatial attention module, '$\sigma(\cdot)$' represents sigmoid function, '$\text{MLP}(\cdot)$' represents
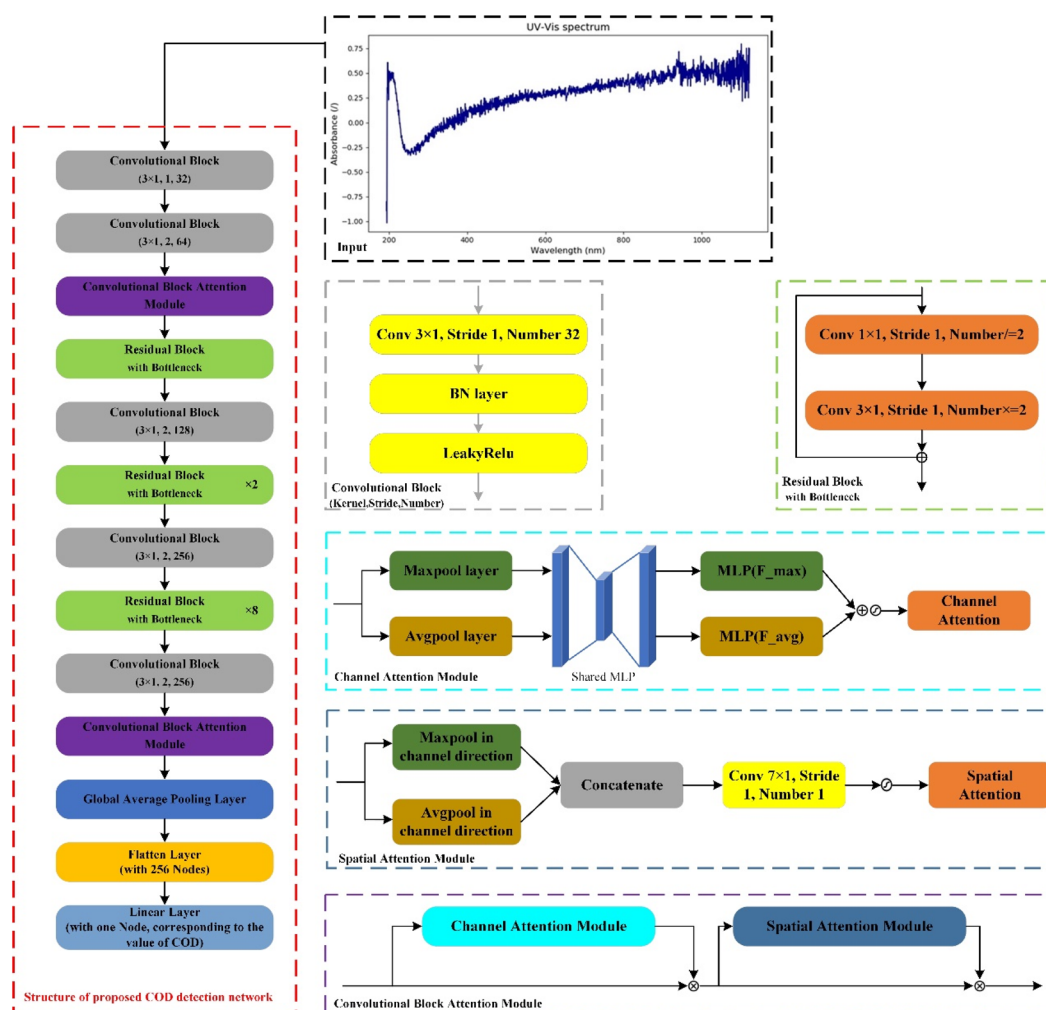

Fig. 4 The structure of proposed COD detection network.

multilayer perceptron, '[·; ·]' represents concatenate operation on channel dim.

The role of CBAM is adaptive refinement of spectral features. Since different water quality parameters in water samples have sensitive bands in the UV-Vis spectrum, for example: the sensitive band for turbidity is 380–740 nm, the sensitive band for chroma is 390–440 nm, and the sensitive band for TOC (*Total Organic Carbon*) is 250–390 nm. Our goal is to increase representation power by using attention mechanism: focusing on important features that affect COD and suppressing unnecessary ones. Therefore, we applied CBAM, so that neural network can know "where" (spatial attention modules) wavelength features has an impact on output, and "what" (channel attention modules) channel has the greatest impact on output.

In addition, in this network, the last three layers are:

1. Global average pooling layer: select the average value in each feature map as the output of this channel.

2. Flattening layer: flatten the feature map into a 256-dimensional vector.

3. Linear layer: there is only one output node, corresponding to the COD square root value.

2.9 Early-stopping and model-checkpoint

Early-stopping is used to monitor validation loss and halts the training when validation accuracy does not improve after a certain number of epochs (in this work, a patience epoch = 5). This strategy prevents overfitting because it stops training when the performance of the validation set starts to decline. Moreover, the weights of the model at its peak performance are restored by model-checkpoint. This ensures that the best model is retained at the end of the training rather than the final model.[24,25]

2.10 Workflow of COD detection

In order to apply the proposed method to COD detection in real water, we designed an automated detection module, as shown in Fig. 5(C).

The automated detection module is placed in the water quality dynamic detecting equipment and mainly includes the following components:

1. Detection room. Container for storing water samples to be tested.

2. Spectrometer. Deuterium halogen lamps are selected as light sources to produce stable intensity light.

3. Optical attenuator. Used to minimize signal distortion and improve equipment reliability.

4. Water pump. Used to draw water samples into the detection room and discharge the water samples in the detection room.

5. Locating mechanism. Used to fix the position and posture of the above components.

The workflow diagram of the automatic detection module is shown in Fig. 6. Among them, the control circuit is used to implement the mechanical operation and control logic of the module, such as pumping water samples, draining water samples, power on the industrial computer, *etc.* Industrial computer is mainly used to collect UV-Vis spectrum, such as setting operating parameters, calculating absorbance, transmitting spectral data to the server, *etc.* The server is used to accept the raw UV-Vis spectrum uploaded by the automatic
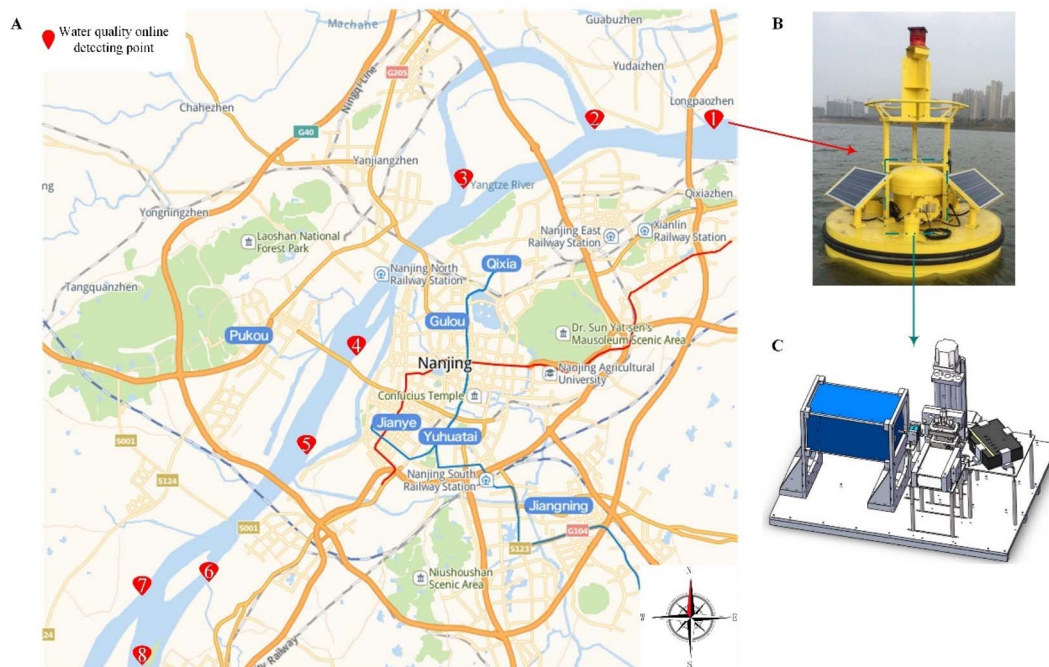

Fig. 5 Equipment design and deployment for COD detection in actual waters. (A) Schematic diagram of the distribution of water quality online detecting points taking Nanjing City, Jiangsu Province, China as an example. (B) Water quality dynamic detecting equipment. (C) Structure design of our COD online detection module.
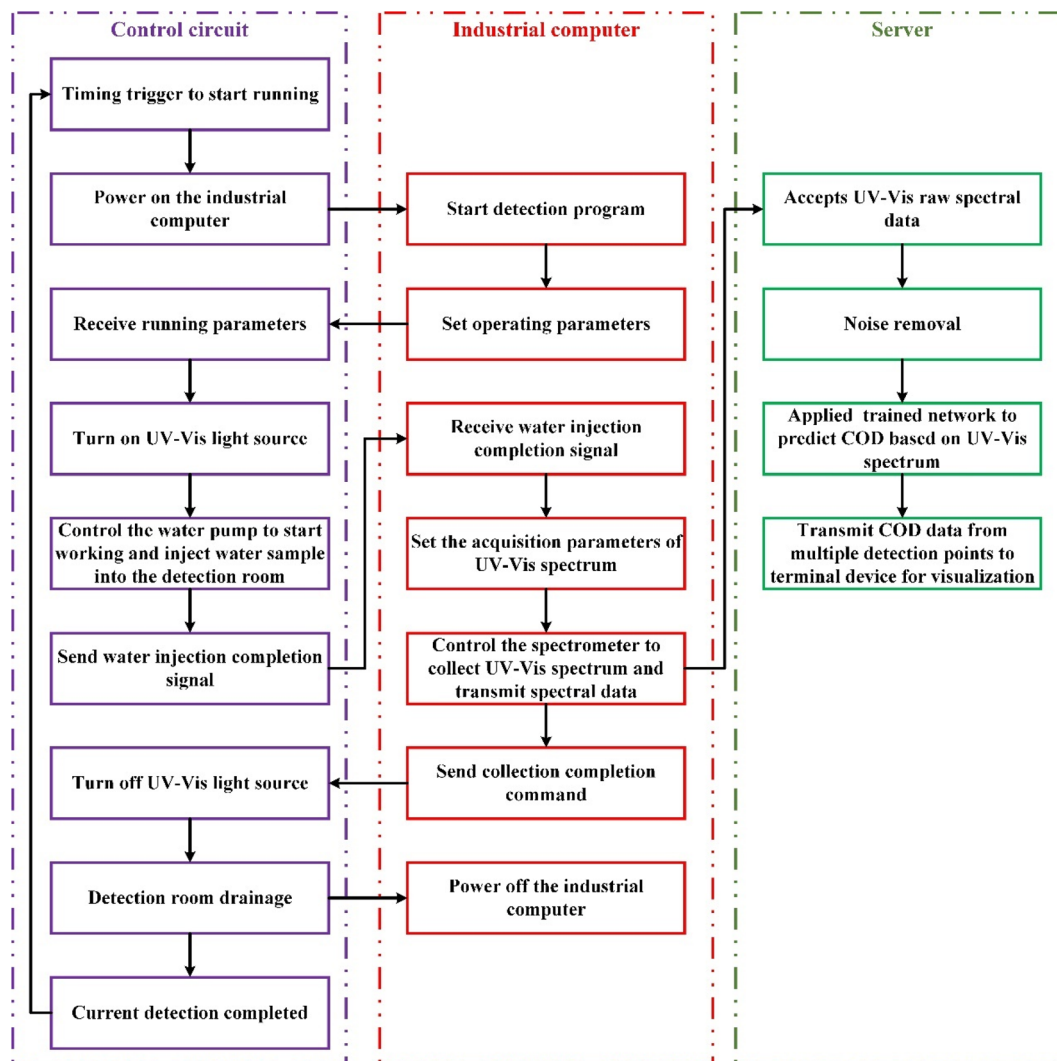
Fig. 6 Work flow chart of the automated detection module in water quality dynamic detecting equipment.

detection module in each sampling point, use the deployed neural network to detect COD, then combine the sampling point location and the corresponding COD value for visualization, and finally send the data to the terminal for rendering.

UV-Vis spectroscopy for COD prediction of surface water is a detection method that uses absorption characteristics of organic matter or part of inorganic matter in water to calculate COD value of water sample from absorption spectrum. The specific steps of data set construction, model training and testing are shown in Fig. 7.

2.11   Algorithm running environment

The computer configuration parameters used for neural network model training and testing are shown in Table 2.

3.   Results

3.1   Training

The convolutional layers were pretrained on LAMOST Spectra 4-class classification dataset.[26] For pretraining we use the first 17

convolutional layers from Fig. 4 followed by a Flatten layer and a SoftMax layer. This network was pretrained for approximately 2 hours on RTX4080 and achieve a top-1 accuracy of 96% on the validation set.

A leaky rectified linear activation is used after each convolutional layer, which is shown in formula (11).

$$\varnothing(x) = \begin{cases} x, & \text{if } x > 0 \\ 0.05x, & \text{otherwise} \end{cases} \qquad (11)$$

Then the model is converted to perform COD detection. We fixed the weights for the first 17 convolutional layers and only trained the weights for last two linear layers.

The mean squared error[27] is used to optimize our model. But mean squared error doesn't exactly match our training goals. It gives equal weight to large COD and small COD errors. Our error measure should reflect that small deviations from large COD are more important than small deviations from small COD. To partially solve this problem, we predict the square root of COD instead of predicting COD directly.
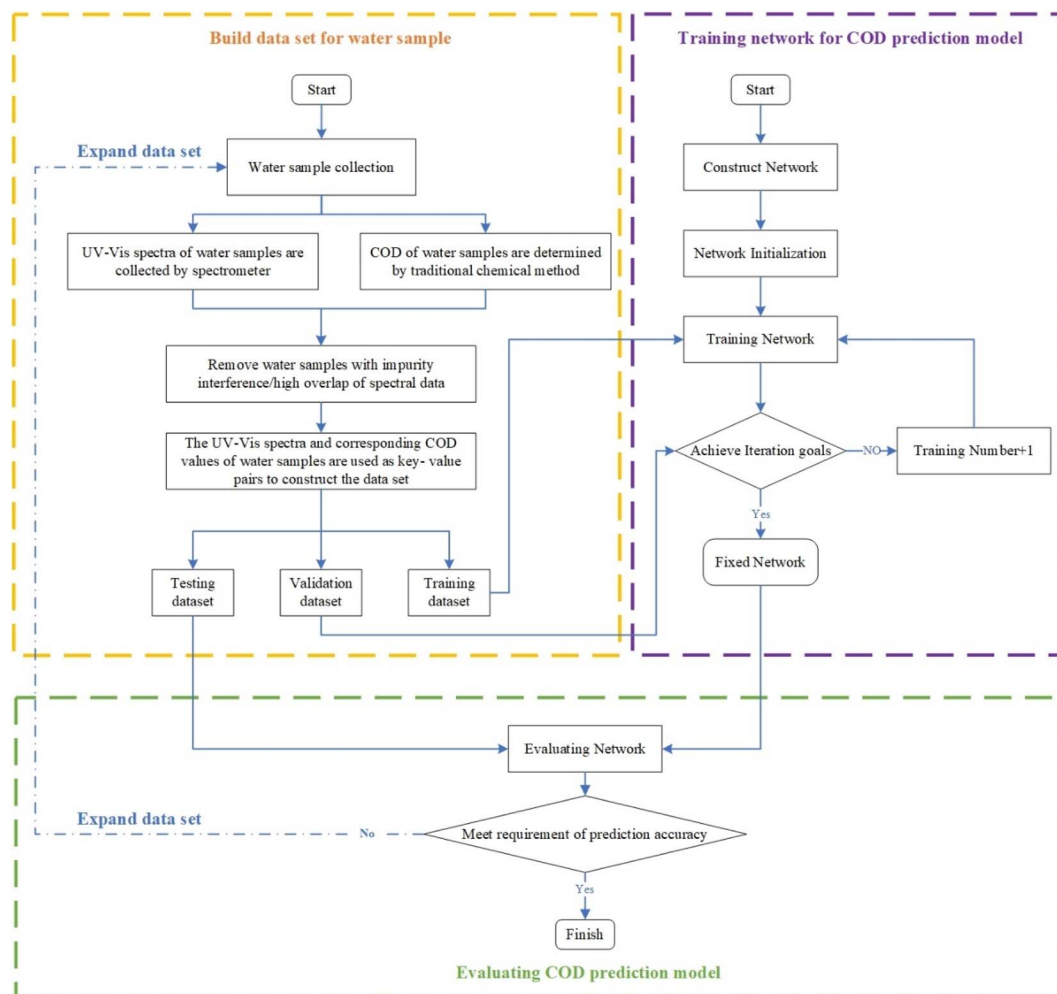
Fig. 7 Work flow chart of spectral preprocessing, model training and model evaluating.

Table 2 Algorithm running environment

OS	CPU	GPU	Pytorch-gpu	Python	Anaconda
Windows 11	i7-13700KF	RTX4080	2.0.1+cu118	3.10.11	23.3.1

To sum up, our loss function is shown as formula (12).

$$\text{Loss} = \frac{1}{M} \sum_{\substack{i=1, \\ p_i \in D_{\text{lamost}}}}^{M} p_i \times \log \widehat{p_i} + \frac{1}{N} \sum_{\substack{k=1, \\ y_k \in D_{\text{cod}}}}^{N} \left(\sqrt{y_k} - \sqrt{\widehat{y_k}} \right)^2 \quad (12)$$

where cross entropy error is used to optimize our model in pretrained on D_{lamost} classification dataset.

We train the network for 155 epochs on the training dataset and evaluate on validation dataset. To optimize the training process, the initial learning rate is set as 10^{-3}, and we decay the learning rate of each parameter group by 0.8 times every 5 epochs. Throughout training, we use optimizer of 'Adam', a batch size of 32, epochs of 160. The network convergence process is shown as Fig. 8(A).

In order to investigate the generalization ability of the network, the network prediction evaluation on the validation dataset is set every epoch, results are shown in Fig. 8(B). As can be seen that the network has strong generalization ability, in the validation dataset, the relative error of 99.54% COD prediction results is within 10%, and that of 90.36% COD prediction results is within 5%.

3.2 Inference

Generalization refers to the ability of a model to digest new data and make accurate predictions after training on the training set.

To verify the generalization ability of the proposed model, we introduce Pearson correlation coefficient[28] to measure the linear correlation between the predicted COD value and the true COD value. The Pearson correlation coefficient formula is shown in formula (13).

$$R = \sum_{k=1}^{N} (y_k - \bar{y})(t_k - \bar{t}) \left/ \sqrt{\sum_{k=1}^{N} (y_k - \bar{y})^2 \sum_{k=1}^{N} (t_k - \bar{t})^2} \right. \quad (13)$$

where 'N' represents the number of water samples in dataset, 'y_k' represents COD ground-truth on sample k, '$\bar{y}$' represents the
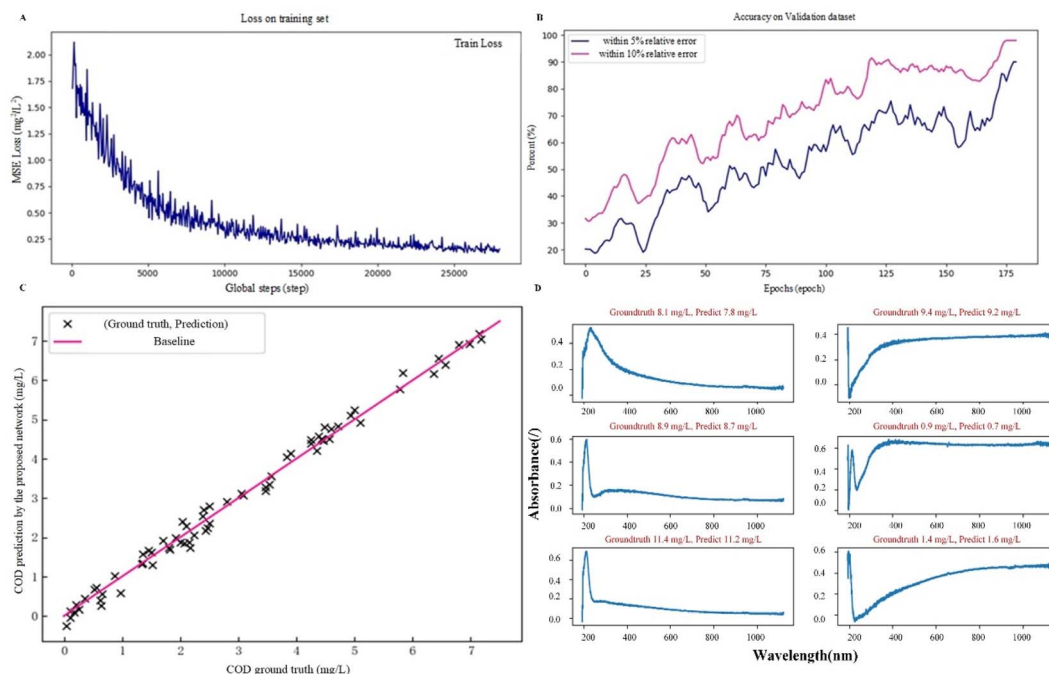

Fig. 8 Performance of the model during training, validation and testing. (A) Convergence process on training dataset. (B) Generalization ability on validation dataset. (C) Generalization ability on testing dataset. (D) The test results of complete COD detection model.

mean value of COD ground-truth, 't_k' represents COD prediction by proposed network on sample k, '$\bar{t}$' represents the mean value of COD prediction.

As shown in formula (13), the closer the Pearson correlation coefficient of proposed model is to 1, the closer the predicted value is to the ground truth, and the stronger the generalization ability of the model. We fixed the network weights and using 67 groups new data to verify the generalization ability. The results are shown as Fig. 8(C), and the Pearson correlation coefficient has a value of 0.97.

We pipelined the noise removal algorithm in section 2.5 and prediction network in section 2.7 to form a complete COD detection model in this paper.

We randomly selected 6 samples' raw UV-Vis absorption spectrum from the 67 groups new data, and input them into proposed COD detection model. The predicted value and corresponding ground truth are shown in Fig. 8(D).

As shown in Fig. 8, the proposed COD detection model has a good performance on both noise tolerance and accuracy.

4. Discussion

4.1 The role of noise removal

At present, the research on COD detection mainly focuses on improving accuracy.[5,7,10,11,28] And many scholars directly transmit raw spectrum with noise to the neural network for end-to-
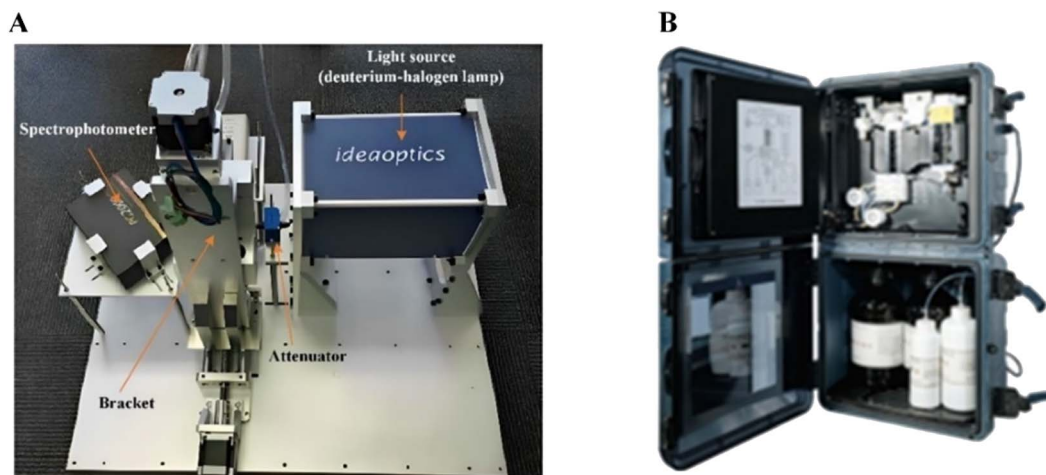

Fig. 9 COD online detection device. (A) The prototype of the COD online detection device we designed. (B) CODmax III (Online COD detector produced by HACH company).

end training. In our previous work, we also trained the end-to-end network under specific detection scenarios. Experiments show that under ideal circumstances, the end-to-end network has better generalization ability and can obtain better fitting results. However, in this paper, we still choose the two-stage strategy for the following reasons:

4.1.1 Interpretability. Currently, many of the spectroscopic datasets used in research are collected in specific laboratory environment, using the equipment shown in Fig. 2(A). However, when designing COD online detection equipment, the overall size and weight, equipment reliability and waterproofing need to be considered comprehensively, the design is often shown in Fig. 9. This means that the environment noise under actual working conditions is much greater than that under laboratory conditions. We hope to restore the spectral data with high SNR corresponding to the spectrum collected under working conditions, so as to eliminate the influence caused by noise to the measurement.

4.1.2 Reusability. In addition to predicting COD, UV-Vis spectrum with high SNR can also be used to measure DOP (Dissolved Organic Phosphorous) and DON (Dissolved Organic Nitrogen). Therefore, many programmers hope to directly obtain the denoised UV-Vis spectrum.

However, few research[9,13] carry out the universal detection framework of COD based on the real water sample spectrum with low Signal to Noise Ratio (SNR).

To discuss the role of noise removal in this work, the performance of multiple algorithms was tested simultaneously on a new water sample dataset. The results are shown in Table 3.

As shown in Table 3, the spectrum preprocessing can effectively improve the accuracy of the model. However, the denoising autoencoder is difficult to effectively remove noise, possibly due to the high redundancy of the UV-Vis spectrum and the insufficient amount of training data. We believe the theoretical reasons that may be related to the network model are as follows:

It is difficult for a purely data-driven neural network to learn the distribution pattern of noise under the current scale of the data set. Fluctuations in the output power of the light source, doping of the optical fiber material, particles in the CCD module and environmental vibration are the main causes of spectral noise, which is represented by the burr of high

Table 3 Performance of different detection algorithms based on UV-Vis spectroscopy

Noise removal algorithm	COD prediction method	End to end	Spectra region	R
None	PLS	Yes	220 nm, 253 nm	0.68
None	SVR	Yes	220 nm, 253 nm	0.70
None	ANN	Yes	200–762 nm	0.64
None	CNN	Yes	200–762 nm	0.66
None	VGG	Yes	200–762 nm	0.66
None	ResNet18	Yes	200–762 nm	0.70
None	**Proposed network**	Yes	200–762 nm	**0.75**
Hard threshold noise filter	PLS	No	220 nm, 253 nm	0.75
Hard threshold noise filter	SVR	No	220 nm, 253 nm	0.76
Hard threshold noise filter	ANN	No	200–762 nm	0.71
Hard threshold noise filter	CNN	No	200–762 nm	0.69
Hard threshold noise filter	VGG	No	200–762 nm	0.72
Hard threshold noise filter	ResNet18	No	200–762 nm	0.79
Hard threshold noise filter	**Proposed network**	No	200–762 nm	**0.84**
Soft threshold noise filter	PLS	No	220 nm, 253 nm	0.76
Soft threshold noise filter	SVR	No	220 nm, 253 nm	0.76
Soft threshold noise filter	ANN	No	200–762 nm	0.70
Soft threshold noise filter	CNN	No	200–762 nm	0.71
Soft threshold noise filter	VGG	No	200–762 nm	0.73
Soft threshold noise filter	ResNet18	No	200–762 nm	0.80
Soft threshold noise filter	**Proposed network**	No	200–762 nm	**0.83**
Proposed threshold filter	PLS	No	220 nm, 253 nm	0.88
Proposed threshold filter	SVR	No	220 nm, 253 nm	0.85
Proposed threshold filter	ANN	No	200–762 nm	0.86
Proposed threshold filter	CNN	No	200–762 nm	0.85
Proposed threshold filter	VGG	No	200–762 nm	0.87
Proposed threshold filter	ResNet18	No	200–762 nm	0.93
Proposed threshold filter	**Proposed network**	No	200–762 nm	**0.97**
Denoising autoencoder	PLS	No	220 nm, 253 nm	0.73
Denoising autoencoder	SVR	No	220 nm, 253 nm	0.74
Denoising autoencoder	ANN	Yes	200–762 nm	0.70
Denoising autoencoder	CNN	Yes	200–762 nm	0.68
Denoising autoencoder	VGG	Yes	200–762 nm	0.71
Denoising autoencoder	ResNet18	Yes	200–762 nm	0.76
Denoising autoencoder	**Proposed network**	Yes	200–762 nm	**0.81**

frequency jumping up and down. For the spectrum of the i-th sample, it is generally assumed that the noise satisfies the Gaussian distribution of fixed mean (μ_i) and fixed variance (σ_i). However, because the spectrum dataset was collected through cooperation between multiple parties, that is, there are different in the types of light sources and spectrometers used by each party, this causes the prior probabilities of μ and σ show a long-tailed distribution for the entire dataset. It is difficult for neural networks based on purely data-driven learning to learn the distribution of μ and σ in the current scale of data sets, resulting in poor prediction results.

4.2 Comparative study

Table 3 also shows the performance of other detection algorithms based on UV-visible spectroscopy.

Among them, PLS and SVR models are commonly used detection methods for COD prediction of water samples in the last century. They are typically characterized by absorbance values at 220 nm and 253 nm as inputs to the model. However, due to the complex composition of real water, the size, type and color of the particles in the water sample will cause varying degrees of interference with the UV-Vis spectrum. This results in a modeling method that uses only a few characteristic bands as input, making it difficult to accurately predict the COD value in actual water samples.

On the other hand, data-driven detection methods such as ANN, CNN and VGG often use the full-band spectrum as the input of the model for modeling. Although this type of deep learning model has strong generalization capabilities, when the amount of data in the training set is insufficient and the linear redundancy of the spectrum is high, it can easily lead to overfitting, thus reducing the accuracy of prediction.

However, the ResNet18 alleviates the problems of degradation and overfitting by shortcut connection and dropout layer. As shown in Table 3, on the basis of ResNet18, the prediction model proposed in this work introduces the attention mechanism, which ensures the model nonlinear fitting ability, further alleviates the overfitting problem of deep learning, and thereby improves detection accuracy.

In addition to UV-Vis spectrum, the fluorescence spectrum (also known as excitation–emission matrix) can obtain the complete spectral information of fluorophores in humus, and other organic matter such as lignin, plankton, proteins, and some aliphatic groups can also emit fluorescence. Therefore, fluorescence spectroscopy can also be used for online COD detection.

The diaphragm electrode method, on the other hand, uses electrodes to detect the amount of oxygen as it passes through a highly oxygen permeable diaphragm and is widely used to measure dissolved oxygen levels. Moreover, there is a negative correlation between dissolved oxygen and COD. Therefore, after fitting the relationship between dissolved oxygen and COD through polynomial, COD can also be measured indirectly through the diaphragm electrode method.

In order to further demonstrate the superiority of the proposed method over previous methods, we conducted a comparative study, as shown in Table 4.

Table 4 also provides detailed data processing associated with these methods, such as data preprocessing, modeling, initial parameter settings and final measurement accuracy.

From the perspective of automated design and product maintenance, we believe that compared with diaphragm electrode method, the detection mechanisms of fluorescence spectroscopy and UV-Vis spectroscopy are more suitable for online COD detection in real water. Therefore, the main comparative work was placed on fluorescence spectroscopy. In addition, as shown in Table 4, the proposed method has better performance compared with other previously reported methods.

4.3 Performance experiments of detection method

In addition to using the Pearson correlation coefficient to measure the accuracy of the proposed method, we also conducted the following performance tests on the proposed method in accordance with the relevant definitions of the *International Union of Pure and Applied Chemistry* on chemical detection methods:

4.3.1 LOD (limit of detection). Its expression is shown in formula (14).

$$x_{\mathrm{L}} = \bar{x}_{\mathrm{b1}} + k s_{\mathrm{b1}} \tag{14}$$

Table 4 Comparative study between the proposed method and previously reported methods

Measurement method	Noise removal method	Modeling method	Initial parameters[a]	Measurement accuracy	
				MSE (mg^2 L^{-2})	R
Fluorescence spectroscopic	Smoothness	Polynomial fitting	$n = 3$	0.49	0.91
	Smoothness	SVM	$c = 1.4, \sigma = 0.37$	0.35	0.94
	Smoothness	LS-SVM	$\gamma = 13, \sigma = 0.68$	0.41	0.92
	DWT	Polynomial fitting	$n = 3$	0.55	0.90
	DWT	SVM	$c = 1.4, \sigma = 0.37$	0.34	0.94
	DWT	LS-SVM	$\gamma = 13, \sigma = 0.68$	0.38	0.93
Diaphragm electrode	None	Polynomial fitting	$n = 3$	0.22	0.96
Proposed method	Proposed threshold filter	Proposed network	Fixup initialization	0.18	0.97

^{a} n represents the highest power of the polynomial, c represents the punishment coefficient, σ represents the kernel function parameter, γ represents the regularization parameter.

In the formula (14), x_L represents the detection limit of the equipment, $\bar{x}_{b1}$ represents the blank mean value, k is the domain confidence-related constant, and the usual value is 3. s_{b1} is the standard deviation of the blank value. The standard deviation calculation formula is as formula (15).

$$s_{b1} = \sqrt{\frac{\sum_{i=1}^{n}(x_i - \bar{x})^2}{n-1}} \quad (15)$$

In the formula (15), n represents the number of measurements, and the usual value is 20, $\bar{x}$ is the average measurement value of the equipment corresponding to the blank value, x_i represents the i-th measurement value.

The redistilled water was used as the index blank solution and measured 20 times continuously. Through experiments, the detection limit of this method is 0.07 mg L^{-1}.

4.3.2 Range test. Referring to the relevant regulations of *Japanese Industrial Standards*, set the lower limit of the measuring range to 10 times the detection limit. Therefore, the lower limit of the measuring range is: 0.70 mg L^{-1}. The upper limit of the measuring range refers to the maximum value that the equipment can detect under certain accuracy conditions. Therefore, we set the maximum relative error to 5%. Through multiple experiments, we can find that the measuring range of this detection method is 0.70–15.00 mg L^{-1}.

4.3.3 Zero drift test. Zero drift is the continuous change of the zero-point indication value within a period of time caused by changes in measurement characteristics. We used double-distilled water as the zero-point calibration solution, made the equipment continuously test for 24 hours, and calculated the percentage of the maximum change amplitude relative to the range value. Its expression is shown in formula (16).

$$ZD = \frac{|\max(x_i) - x_0|}{l_{nw}} \times 100\% \quad (16)$$

In the formula (16), $\max(x_i)$ represents the maximum value measured within 24 hours, x_0 represents the measured value at the initial detection time point, l_{nw} represents the range of the device. Through experiments, the zero drift of this method is 0.94%.

4.3.4 Repeatability testing. Repeatability characterizes measurement precision under the same measurement conditions. Relative Standard Deviation (abbreviated as RSD) is usually used in chemical testing to express the consistency of results, and its expression is shown in formula (17).

$$ZD = \frac{|\max(x_i) - x_0|}{l_{nw}} \times 100\% \quad (17)$$

In the formula (17), x_i represents the i-th measurement value, $\bar{x}$ represents the average measurement value, n represents the total number of measurements, and $n \geq 6$ is often required. Through experiments, the highest RSD value of this method is 1.89%.

5. Conclusion

In summary, we have proposed and developed an improved online COD prediction measurement. The main work contents include: design the structure and workflow of online automatic detection module, propose an improved noise removal method for UV-Vis spectrum, and propose a COD detection network based on deep learning. The main findings of the paper are as follow:

1. The DWT denoising algorithm based on the improved threshold function (the denoising method proposed in this paper) preprocesses the UV-Vis spectrum of water samples, which can effectively improve the accuracy of subsequent detection models. Through a large number of comparative experiments, it was found that the Pearson correlation coefficient (R) of the proposed denoising method can be increased by 21.4% to 29.3% compared to not using the denoising algorithm. In addition, compared with the denoising autoencoder, the proposed denoising method can increase the R by 15.2% to 19.8%. Indicates that the proposed denoising method is more suitable for UV-Vis spectrum.

2. The COD detection network (proposed in this paper) composed of the residual module and the CBAM module can improve the detection accuracy, and the R in the test set is 0.97. Compared with the SVM model, it has improved by 12%, and compared with ResNet, it has improved by 4%.

3. For the trained COD prediction network, 90.36% of the prediction results have a relative error within 5%, and 99.54% of the COD prediction results have a relative error within 10%. In addition, the MSE (mean squared error) of the network on testing set is 0.18, while the fluorescence spectroscopic method is 0.35–0.55, and the diaphragm electrode method is 0.22. It shows the proposed method has better performance compared with other previously reported methods.

4. Through the performance experiments of the detection method, it can be seen that the detection limit of the proposed method is 0.07 mg L^{-1}, the measuring range is 0.70–15.00 mg L^{-1}, the zero drift is 0.94%, and the repeatability is 1.89%

Conflicts of interest

There are no conflicts of interest to declare in this work.

Acknowledgements

References

1 Z. Zhang, F. Xia, D. Yang and Y. Chen, Discussion of an environmental depletion assessment method-A case study in Xinjiang, China, *PLoS One*, 2022, **17**(1), e0262092.

2 L. Wu, X.-W. Qiu, T. Wang, K. Tao, L.-J. Bao and E. Y. Zeng, Water Quality and Organic Pollution with Health Risk Assessment in China: A Short Review, *ACS ES&T Water*, 2022, **2**(8), 1279–1288.

3 M. Zhong, T. Wang, W. Zhao, J. Huang, B. Wang, L. Blaney, *et al.*, Emerging Organic Contaminants in Chinese Surface Water: Identification of Priority Pollutants, *Engineering*, 2022, **11**(4), 111–125.

4 M. Lepot, A. Torres, T. Hofer, N. Caradot, G. Gruber, J.-B. Aubin, *et al.*, Calibration of UV/Vis spectrophotometers: A review and comparison of different methods to estimate TSS and total and dissolved COD concentrations in sewers, WWTPs and rivers, *Water Res.*, 2016, **101**, 519–534.

5 J. L. McHale, *Molecular Spectroscopy*, CRC Press, 2nd edn, 2017.

6 M. Xia, R. Yang, G.-f. Yin, X. Chen, J. Chen and N. Zhao, A method based on a one-dimensional convolutional neural network for UV-vis spectrometric quantification of nitrate and COD in water under random turbidity disturbance scenario, *RSC Adv.*, 2022, **13**(1), 516–526.

7 Y. Zhao, H. Wang, Z. Liu, Y. Li and S. Fan, Novel method for on-line water COD determination using UV spectrum technology, *Chin. J. Sci. Instrum.*, 2010, **31**(9), 1927–1932.

8 J. Agustsson, O. Akermann, D. A. Barry and L. Rossi, Non-contact assessment of COD and turbidity concentrations in water using diffuse reflectance UV-Vis spectroscopy, *Environ. Sci.: Processes Impacts*, 2014, **16**(8), 1897–1902.

9 Z. Wang, Y. Man, Y. Hu, J. Li, M. Hong and P. Cui, A deep learning based dynamic COD prediction model for urban sewage, *Environ. Sci.: Water Res. Technol.*, 2019, **5**(3), 124–131.

10 Y. Jiang, C. Li, L. Sun, D. Guo, Y. Zhang and W. Wang, A deep learning algorithm for multi-source data fusion to predict water quality of urban sewer networks, *J. Cleaner Prod.*, 2021, **3**(8), 128–133.

11 J. Li, Y. Tong, L. Guan, S. Wu and D. Li, A turbidity compensation method for COD measurements by UV–vis spectroscopy, *Optik*, 2019, **186**, 129–136.

12 A. A. Babaei and F. Ghanbari, COD removal from petrochemical wastewater by UV/hydrogen peroxide, UV/persulfate and UV/percarbonate: biodegradability improvement and cost evaluation, *J. Water Reuse Desalin.*, 2016, **6**(4), 484–494.

13 S. Zhao, G. Huang, G. Cheng, Y. Wang and H. Fu, Hardness, COD and turbidity removals from produced water by electrocoagulation pretreatment prior to Reverse Osmosis membranes, *Desalination*, 2014, **344**, 454–462.

14 S. M. Ahmed, A. Al-Shrouf and M. Abo-Zahhad, ECG data compression using optimal non-orthogonal wavelet transform, *Med. Eng. Phys.*, 2000, **22**(1), 39–46.

15 J. Li, Y. Tong, L. Guan, S. Wu and D. Li, A UV-visible absorption spectrum denoising method based on EEMD and an improved universal threshold filter, *RSC Adv.*, 2018, **8**(16), 8558–8568.

16 *You Only Look Once: Unified, Real-Time Object Detection*, Redmon J., Divvala S., Girshick R. and Farhadi A., Computer Vision & Pattern Recognition, 2016.

17 P. Jiang, D. Ergu, F. Liu, Y. Cai and B. Ma, A Review of Yolo Algorithm Developments, *Procedia Comput. Sci.*, 2022, **199**, 7.

18 *Image Super-Resolution via Deep Recursive Residual Network*, Tai Y., Yang J. and Liu X., IEEE Conference on Computer Vision & Pattern Recognition, 2017.

19 Z. Liu, J. Du, M. Wang and S. S. Ge, ADCM: Attention Dropout Convolutional Module, *Neurocomputing*, 2020, **394**, 95–104.

20 *Rotate to Attend: Convolutional Triplet Attention Module*, Misra D., Nalamada T., Arasanipalai A. U. and Hou Q., IEEE/CVF winter conference on applications of computer vision, 2020.

21 A. Veit, M. Wilber and S. Belongie, Residual Networks Behave Like Ensembles of Relatively Shallow Networks, *Adv. Neural Inf. Process. Syst.*, 2016, **29**, 55–61.

22 S. H. Wang, Q. Zhou, M. Yang and Y. D. Zhang, ADVIAN: Alzheimer's Disease VGG-Inspired Attention Network Based on Convolutional Block Attention Module and Multiple Way Data Augmentation, *Front. Aging Neurosci.*, 2021, **13**, 687–696.

23 *CBAM: Convolutional Block Attention Module*, Woo S., Park J. and Lee J. Y., European conference on computer vision, 2018.

24 N. Nehra, P. Sangwan and D. Kumar, Artificial Neural Networks: A Comprehensive Review, *Handbook of Machine Learning for Computational Optimization*, 2021.

25 *Mechanism of Overfitting Avoidance Techniques for Training Deep Neural Networks*, Sabiri B., Asri B. E. and Rhanoui M., International Conference on Enterprise Information Systems, 2022.

26 F. Yang, L. Deng, C. Liu, J. L. Carlin, H. J. Newberg, K. Carrell, *et al.*, Hydrogen lines in LAMOST low-resolution spectra of RR Lyrae stars, *New Astron.*, 2014, **26**, 72–76.

27 Z. Wang and A. C. Bovik, Mean squared error: Love it or leave it? A new look at Signal Fidelity Measures, *IEEE Signal Process. Mag.*, 2009, **26**(1), 98–117.

28 J. L. Rodgers, W. A. Nicewander and D. C. Blouin, Thirteen ways to look at the correlation coefficient, *Am. Stat.*, 1988, **42**(1), 59–66.